Chapter 5

The Multi-Strip Coupler and Its Applications

The multi-strip coupler, first demonstrated by Marshall and Paige [113], consists of an array of identical electrodes oriented parallel to the surface-wave wavefront. The electrodes are electrically disconnected. As already mentioned in Chapter 1 the coupler may be used to transfer the surface wave power laterally, so that the output wave occupies a track displaced relative to that of the input wave, as in Figure 1.2. In many devices the coupler is used in this way to couple two interdigital transducers whose active regions do not overlap. This arrangement has the practical merit that spurious output signals due to excitation of bulk waves are much reduced, and the device response is easily calculated even if both transducers are apodised, thus introducing additional design flexibility. There are also many modified forms of the coupler with diverse applications, giving in particular several methods of reducing the level of spurious triple-transit signals in surface-wave devices. The number of electrodes required in the coupler depends inversely on the piezoelectric coupling strength of the substrate material, and for this reason the coupler is practicable only for strongly piezoelectric materials such as lithium niobate.

The basic mechanism of the coupler is a straightforward application of the piezoelectric effect. A surface wave incident in one track causes voltages to be induced on the electrodes, which therefore apply voltages in the second track, generating a second surface wave there. At any frequency, the induced voltages have relative phases corresponding to the propagating surface wave, so that waves generated by individual electrodes in the second track will be in phase. It is thus clear that the coupler will have a wide bandwidth, much wider than that of a transducer with a comparable length.

A quantitative description can be obtained by considering the propagating modes of the structure, that is, solutions in which all the field variables, such as the surface potential $\phi(x)$, have the property $\phi(x + p) = \phi(x) \exp(-jkp)$, where k is some wavenumber and p is the pitch. A solution such as this is found to exist for a uniform surface-wave beam, with the electrodes extending over the width of the beam. When two tracks are coupled by a set of electrodes, it is found that the basic solution splits into two modes with slightly different wavenumbers. A simple coupler, with identical geometries in the two tracks, gives a symmetric mode and an anti-symmetric mode;

the former has the surface-wave amplitudes the same in both tracks, while the latter has the amplitudes the same except for being opposite in sign. For a wave incident in one track, the waves in the coupler are readily found by superimposing the two modes, as will be shown in Section 5.2. It is found that the surface-wave energy is completely coupled from one track to the other in a distance related to the velocity difference of the symmetric and anti-symmetric modes, and that the waves in the two tracks have a phase difference of $\pi/2$. This behaviour is similar to many other systems involving weakly-coupled waves, for example waves in weakly-coupled waveguides. Another example is surface-wave propagation on a substrate of finite thickness, considered in Section 2.2.5.

To find the basic modes of the coupler, it is first necessary to consider propagation in an infinite array of electrodes, taking the surface-wave amplitude to be uniform in the transverse direction. Here the structure is periodic, and the wave properties show features in common with many other waves in periodic structures, for example electron waves in crystals and electromagnetic waves in a helix. A comprehensive review is given by Elachi [114]. The wave motion is evanescent if the frequency is within one of a set of bands known as stop bands. The stop bands are centred approximately at the frequencies where the pitch of the structure equals a multiple of the half-wavelength. This is readily appreciated if the structure is modelled as an array of weakly-reflecting elements, and Appendix E gives further details of this model, showing that the width of the stop bands is related to the reflection coefficient. The same conclusions can be obtained from coupled wave analysis [114]. Rigorous anlaysis is often facilitated by Floquet's theorem, which states that the amplitude of a propagating wave can be expressed as an infinite series with terms of the form $\exp[-j(k + 2\pi n/p)x]$, where p is the pitch of the structure. The individual terms are called space harmonics.

In most practical couplers the number of electrodes is large, and so end effects are not significant. Consequently, the results for a periodic structure may be applied directly to a coupler of finite length. An analysis using perturbation theory has been given by Maerfeld *et al.* and applied to a wide variety of cases [115–118]. An alternative, and very general, method given by Bløtekjaer *et al.* [119, 120] uses Floquet's theorem and the effective permittivity $\varepsilon_s(\beta)$ discussed in Chapter 3. For coupling to Rayleigh waves, Ingebrigtsen's approximation for $\varepsilon_s(\beta)$ is used, and the results are equivalent to the perturbation analysis. This is described in Appendix D.

The analysis given here is based on the quasi-static Green's function method, using equations given in Section 4.3. This method is relatively straightforward. The quasi-static approximation neglects electrode interactions, and this has the consequence that the stop bands are not predicted, and there are small errors in the predicted surface-wave velocities. However, for most practical devices, designed to operate outside the coupler stop bands, these errors are of little consequence. The analysis is subject to the assumptions made in deriving the equations of Section 4.3, so that the only acoustic wave present is assumed to be a piezoelectric Rayleigh wave. Mechanical loading and the resistivity of the electrodes are assumed to be negligible.

Section 5.1 gives the analysis for an infinite array of electrodes, with the surface-wave amplitude uniform in the transverse direction. This analysis is needed to

establish the basic modes of a coupler. In particular, the solutions for shorted and for open-circuited electrodes give the symmetric and anti-symmetric modes for the basic form of coupler. The coupler itself is first considered in Section 5.2. Section 5.3 considers the use of the coupler to couple two interdigital transducers, the commonest application. The remaining sections describe a variety of other applications, involving modified forms of the coupler.

5.1. ANALYSIS FOR AN INFINITE ARRAY OF ELECTRODES

We first consider an infinite array of regular electrodes with pitch p and width a, as shown in Figure 5.1. The electrode length, W, in the y-direction is assumed to be large, so that all the field quantities can be taken to be independent of y over the electrodes. The origin for the x-axis is at the centre of one electrode, and the voltage on the electrode centred at $x = np$ is V_n, while the current entering this electrode is I_n. We consider specifically solutions in which the voltages and currents can be written

$$V_n = V_0 \exp(-j\kappa np) \tag{5.1a}$$

and

$$I_n = I_0 \exp(-j\kappa np), \tag{5.1b}$$

where a factor $\exp(j\omega t)$ is implicit. The constant κ is arbitrary at this stage, though it should be noted that the solution is unaffected if a multiple of $2\pi/p$ is added to κ. In some particular cases, notably when $V_0 = 0$ or $I_0 = 0$, it will be found that κ can be interpreted as the wavenumber of a perturbed surface wave, with a value close to the free-surface wavenumber k_0. The requirement here is to find a relationship between V_n and I_n and the amplitude of any accompanying surface wave.

The solution is obtained using the quasi-static analysis of Section 4.3. The charge density on the electrodes is dominated by the electrostatic term $\sigma_e(x)$, and by equation (4.33) this can be written in terms of the functions $\varrho_{en}(x)$, defined as the electrostatic charge density when unit voltage is applied to electrode n with other electrodes grounded. In the present case the electrodes are regular, so $\varrho_{en}(x)$ is equal to $\varrho_f(x - np)$, where $\varrho_f(x)$ is the elemental charge density introduced in Section 4.5.1. We thus have

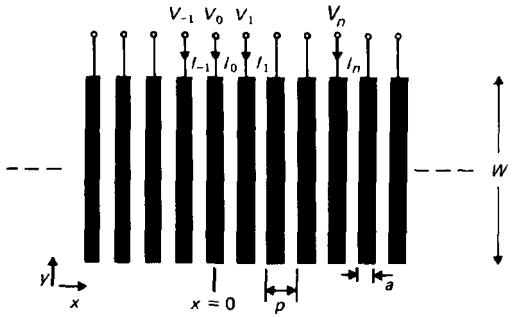

FIGURE 5.1 Infinite array of regular electrodes.

$$\sigma_e(x) = \sum_{n=-\infty}^{\infty} V_n \varrho_{en}(x) = V_0 \sum_{n=-\infty}^{\infty} \varrho_f(x - np)\, e^{-j\kappa np}. \tag{5.2}$$

The Fourier transform of $\sigma_e(x)$ is denoted $\bar{\sigma}_e(\beta)$. Using the shifting theorem, equation (A.10), this is seen to be a sum of complex exponentials, and equation (A.43) shows that this can be written as a sum of delta-functions. With $\bar{\varrho}_f(\beta)$ defined as the Fourier transform of $\varrho_f(x)$, it is found that

$$\bar{\sigma}_e(\beta) = \frac{2\pi V_0}{p} \sum_{m=-\infty}^{\infty} \bar{\varrho}_f(\kappa + 2\pi m/p)\delta(\beta + \kappa + 2\pi m/p), \tag{5.3}$$

where equation (A.24) has been used, and also the symmetry of $\bar{\varrho}_f(\beta)$. The function $\bar{\varrho}_f(\beta)$ is given by equation (4.88).

To find the current I_n entering electrode n, it is first necessary to evaluate the acoustic potential $\phi_a(x, \omega)$, defined as the convolution of the surface-wave Green's function $G_s(x, \omega)$ with $\sigma_e(x)$. It is shown in Section 4.3.4 that $\phi_a(x, \omega)$ may be written in terms of $\bar{\sigma}_e(\beta)$, as in equation (4.47). This equation involves terms proportional to $\bar{\sigma}_e(\pm k_0)$, and terms proportional to $F(\pm k_0)$, which are derived from $\bar{\sigma}_e(\beta)$. In the present case, $\bar{\sigma}_e(\beta)$ is given by equation (5.3), and it can be seen that $\bar{\sigma}_e(\pm k_0)$ is zero unless $\kappa + 2\pi m/p = \pm k_0$ for some m. For the moment this case is excluded; it will be seen later that it occurs when the electrode voltages are zero. Thus, $\phi_a(x, \omega)$ is given by equation (4.47) with the $\bar{\sigma}_e(\pm k_0)$ terms omitted, and with the aid of equation (A.23) this gives

$$\phi_a(x, \omega) = \frac{2\Gamma_s k_0 V_0}{p} \sum_{m=-\infty}^{\infty} \frac{\bar{\varrho}_f(\beta_m) \exp[-j\beta_m x]}{k_0^2 - \beta_m^2}, \tag{5.4}$$

where

$$\beta_m = \kappa + 2\pi m/p. \tag{5.5}$$

Thus $\phi_a(x, \omega)$ has the form of a Floquet expansion.

As in Section 4.3.3, the electrode current I_n can be written

$$I_n = I_{en} + I_{an}, \tag{5.6}$$

where I_{en} and I_{an} are respectively the electrostatic and acoustic contributions. The latter is given by equation (4.43), and since $\varrho_{en}(x) = \varrho_f(x - np)$ we have

$$I_{an} = -j\omega W \int_{-\infty}^{\infty} \varrho_f(x - np)\, \phi_a(x, \omega)\, dx. \tag{5.7}$$

Substituting equation (5.4) for $\phi_a(x, \omega)$ we have

$$I_{an} = -2j\omega W V_n \frac{\Gamma_s k_0}{p} \sum_{m=-\infty}^{\infty} \frac{[\bar{\varrho}_f(\beta_m)]^2}{k_0^2 - \beta_m^2}. \tag{5.8}$$

The electrostatic contribution, I_{en}, is obtained by integrating $\sigma_e(x)$ over the area of electrode n and differentiating with respect to time. This can be expressed in terms of Q_m, the net electrode charges corresponding to the elemental charge density $\varrho_f(x)$, defined in equation (4.89). For voltages V_n on the electrodes, the net charge on electrode n is q_n, given by

$$q_n = W \sum_{m=-\infty}^{\infty} Q_{m-n} V_m = W V_0 \sum_{m=-\infty}^{\infty} Q_{m-n} e^{-jkmp}. \tag{5.9}$$

It is convenient to define a function $C(\kappa)$ by

$$C(\kappa) = \sum_{m=-\infty}^{\infty} Q_m e^{-jkmp} \tag{5.10}$$

so that the electrostatic term is

$$I_{en} = j\omega q_n = j\omega W V_n C(\kappa). \tag{5.11}$$

The function $C(\kappa)$ is derived in Appendix C, equation (C.31), giving

$$C(\kappa) = 2(\varepsilon_0 + \varepsilon_p^T) \frac{\sin(\pi s)}{P_{-s}(-\cos\Delta)} P_{-s}(\cos\Delta), \tag{5.12}$$

where $\Delta = \pi a/p$, and s is defined such that $\kappa p = 2\pi(s + i)$, where i is an integer and $0 \leqslant s \leqslant 1$. The total current is the sum of equations (5.8) and (5.11), so that

$$\frac{I_n}{V_n} = j\omega W \left[C(\kappa) - \frac{2\Gamma_s k_0}{p} \sum_{m=-\infty}^{\infty} \frac{[\bar{\varrho}_f(\beta_m)]^2}{k_0^2 - \beta_m^2} \right]. \tag{5.13}$$

It is convenient to define also ϕ_n as the value of the acoustic potential $\phi_a(x, \omega)$ at $x = np$, and from equation (5.4),

$$\frac{\phi_n}{V_n} = \frac{2\Gamma_s k_0}{p} \sum_{m=-\infty}^{\infty} \frac{\bar{\varrho}_f(\beta_m)}{k_0^2 - \beta_m^2}, \tag{5.14}$$

where $\beta_m = \kappa + 2\pi m/p$.

If $\kappa + 2\pi M/p = \pm k_0$ for some M, we have $\beta_M = \pm k_0$, so that equations (5.13) and (5.14) are both infinite. This case was excluded earlier, but a solution can be obtained by a limiting process, taking the voltages V_n to be zero. For β_M close to $\pm k_0$ the summations are well approximated by omitting all terms except for $m = M$. The ratio of the two equations thus gives the limit

$$I_n = -j\omega W \bar{\varrho}_f(\pm k_0)\phi_n, \quad \text{for } V_n = 0, \tag{5.15}$$

when $\kappa + 2\pi M/p = \pm k_0$. We thus have a solution for all κ. For $V_n = 0$ the solution is consistent with the analysis for a shorted interdigital transducer receiving surface waves, and may be obtained from equation (4.66) of Section 4.4.

For subsequent analysis it is convenient to use an approximate form of the solution. Since the solution is unaffected when $2\pi/p$ is added to κ, we may restrict κ such that the integer parts of $\kappa p/(2\pi)$ and $k_0 p/(2\pi)$ are equal. Thus, for integer i,

$$2\pi i/p \leqslant k_0 \leqslant 2\pi(i + 1)/p, \tag{5.16}$$

and

$$2\pi i/p \leqslant \kappa \leqslant 2\pi(i + 1)/p. \tag{5.17}$$

With this restriction, the summation in equation (5.13) is significant only when κ is close to k_0, and when this is the case the term with $m = 0$ dominates. We may therefore omit the other terms, so that

$$\frac{I_n}{V_n} \approx j\omega W\left[C(\kappa) - \frac{2\Gamma_s k_0}{p}\frac{[\bar{\varrho}_f(\kappa)]^2}{k_0^2 - \kappa^2}\right]. \tag{5.18}$$

Similarly, equation (5.14) becomes

$$\frac{\phi_n}{V_n} \approx \frac{2\Gamma_s k_0}{p}\frac{\bar{\varrho}_f(\kappa)}{k_0^2 - \kappa^2}. \tag{5.19}$$

The potential ϕ_n can be interpreted as the surface wave amplitude at $x = np$. This is justified by the observation that $\phi_a(x, \omega)$ is proportional to $\exp(\pm jk_0x)$ on all unmetallised regions, and therefore gives the surface wave potential in such regions. In the cases of interest here, $\phi_a(x, \omega)$ varies slowly across the width of any one electrode, and hence $\phi_n = \phi_a(np, \omega)$ can be taken as the surface wave amplitude at $x = np$.

Propagation in Shorted or Open-circuited Electrodes The wavenumbers for these two cases are particularly important in the analysis of multi-strip couplers. For shorted electrodes the voltages V_n are zero, and hence equation (5.18) gives $\kappa = k_0$, the wavenumber for propagation on a free surface. This solution was found previously, giving the currents shown by equation (5.15). It is convenient to denote the wavenumber for shorted electrodes by k_{sc}, so that

$$k_{sc} = k_0. \tag{5.20}$$

For open-circuited electrodes the currents I_n are zero. In this case the solution for κ is denoted k_{oc}, and from equation (5.18) we have

$$k_{sc}^2 - k_{oc}^2 = \frac{2\Gamma_s k_0}{p}\frac{[\bar{\varrho}_f(k_{oc})]^2}{C(k_{oc})}. \tag{5.21}$$

Here $\bar{\varrho}_f(k_{oc})$ is given by equation (4.88) of Section 4.5.1, and $C(k_{oc})$ is given by equation (5.12). These functions both vary slowly with k_{oc}. Since k_{oc} must be close to k_0 it is a good approximation to replace k_{oc} by k_0 in these functions. We also have, from equation (3.39) of Chapter 3,

$$\Gamma_s = \frac{1}{\varepsilon_0 + \varepsilon_p^T}\frac{\Delta v}{v} = \frac{1}{\varepsilon_0 + \varepsilon_p^T}\frac{v_0 - v_m}{v_0}, \tag{5.22}$$

where v_0 and v_m are respectively the surface wave velocities for a free surface and for a metallised surface. Equation (5.21) thus gives

$$k_{sc}^2 - k_{oc}^2 = \frac{4k_0}{p}\frac{\Delta v}{v}\frac{\sin(\pi s)}{P_{-s}(-\cos\Delta)P_{-s}(\cos\Delta)}[P_i(\cos\Delta)]^2 \tag{5.23}$$

where i is defined by equation (5.16) and $s = k_0p/(2\pi) - i$.

Equation (5.23) is in agreement with the more rigorous analysis using Floquet's theorem, as shown by equation (D.31) of Appendix D, and also with the results of perturbation theory [118]. However, the theory here predicts that $k_{sc} = k_0$, and does not therefore allow for the perturbation of the surface wave velocity by an array of shorted electrodes. This is one of the consequences of the quasi-static approximation used in the analysis. In practical devices the precise value of k_{sc} is of little consequence, so the above relationships are adequate. A more accurate value for k_{sc} is given in Appendix D, equation (D.26). The above analysis also fails to predict the presence of stop bands. These occur when k_0 is close to multiples of π/p, as shown in Section D.3.

5.2. BASIC COUPLER BEHAVIOUR

In its simplest form the multi-strip coupler is an array of disconnected regular electrodes spanning two identical tracks. In each track the surface wave amplitude is independent of y, but the amplitudes in the two tracks will generally be different. This is illustrated in Figure 5.2. The structure is first analysed as if the number of strips were infinite, and then the results are applied to a finite structure. The pitch p and width a of the electrodes is the same in both tracks, and the two tracks have the same aperture, W.

The electrode voltages and currents are denoted by V_n^a and I_n^a for track A, and by V_n^b and I_n^b for track B. The voltages are the same in the two tracks, and we consider a solution in which they take the form

$$V_n^a = V_n^b = V_0 \exp(-jn\kappa p), \tag{5.24}$$

where the value of κ is taken to be the same for both tracks in view of the restriction imposed by equation (5.17). In addition, continuity of the currents requires

$$I_n^a = -I_n^b. \tag{5.25}$$

These equations give two solutions for propagating waves. The first solution, known as the *symmetric mode*, has the acoustic potentials ϕ_n the same in both tracks. This is the same as the solution for open-circuit electrodes already given in Section 5.1, and therefore gives $\kappa = k_{oc}$. This solution can also be obtained from equations (5.18) and (5.25), which give $I_n^a = I_n^b = 0$.

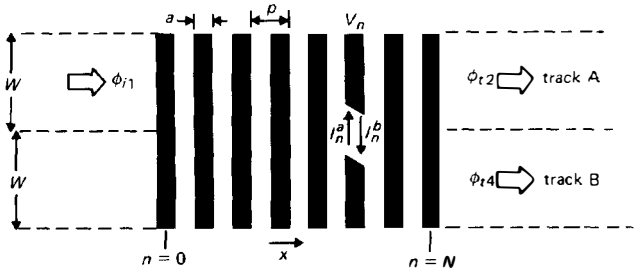

FIGURE 5.2. Simple multi-strip coupler.

The second solution, known as the *antisymmetric mode*, is obtained when the electrode voltages V_n^a and V_n^b are zero. Physically, this is to be expected when the acoustic potentials in the two tracks are equal and opposite. Since the voltages are zero each track will support propagation as if its electrodes were all connected, so that the wavenumber must be $\kappa = k_{sc}$. This solution also follows from equation (5.18), which shows that V_n/I_n is zero when $\kappa = k_0$, which in turn equals k_{sc}. In this case the acoustic potentials are related to the currents by equation (5.15). Denoting the potentials in tracks A and B by ϕ_n^a and ϕ_n^b, we have $\phi_n^a = -\phi_n^b$, since $I_n^a = -I_n^b$.

In order to evaluate the transmission of incident waves by a coupler, it is necessary to consider a more general solution obtained by adding the symmetric and antisymmetric modes. It is sufficient here to take the two modes to have equal amplitudes. denoted by A. The acoustic potentials for the symmetric mode are written

$$\phi_n^a = \phi_n^b = A \exp(-jk_{oc}np)$$

and, for the antisymmetric mode,

$$\phi_n^a = -\phi_n^b = A \exp(-jk_{sc}np).$$

Adding the two modes, the total acoustic potentials are, in track A,

$$\phi_n^a = 2A \cos(\tfrac{1}{2}\pi n/N_c) \exp(-jknp), \tag{5.26}$$

and in track B,

$$\phi_n^b = 2jA \sin(\tfrac{1}{2}\pi n/N_c) \exp(-jknp), \tag{5.27}$$

where $k = (k_{sc} + k_{oc})/2$. The parameter N_c is a function of ω, given by

$$pN_c(\omega) = \pi/(k_{sc} - k_{oc}).$$

Equations (5.26) and (5.27) show that for $n = 0$ the surface wave power is entirely in track A, while for $n = N_c$ the power is entirely in track B. Thus N_c is the number of electrodes required to transfer the surface wave power from one track to the other. N_c may be evaluated using equation (5.23), noting that k_{sc} and k_{oc} are both close to k_0, so that $k_{sc} + k_{oc} \approx 2k_0$. This gives

$$[N_c(\omega)]^{-1} = \frac{\Delta v}{v} \frac{2 \sin(\pi s)}{\pi P_{-s}(-\cos\Delta) \cdot P_{-s}(\cos\Delta)} [P_i(\cos\Delta)]^2, \tag{5.28}$$

where $\Delta v/v$ is the piezoelectric coupling parameter [equation (5.22)], $\Delta = \pi a/p$, i is defined by equation (5.16) and $s = k_0 p/(2\pi) - i$. Thus N_c is inversely proportional to $\Delta v/v$.

Figure 5.3 shows that $N_c(\omega)$ varies slowly with frequency, and has a minimum when $k_0 = \pi/p$, that is, when $\omega = \pi v_0/p$. However, this frequency corresponds to one of the stop bands, and is not therefore used in practice. A typical operating frequency is $\omega = 3\pi v_0/(4p)$. For a metallisation ratio $a/p = \frac{1}{2}$, equation (5.28) gives $N_c = 2.32/(\Delta v/v)$ at this frequency. Thus, for Y, Z lithium niobate, with $\Delta v/v = 2.15\%$, we have $N_c = 108$. At the operating frequency the electrode width is $3\lambda/16$, where λ is the wavelength, and this is somewhat less than the electrode width of $\lambda/4$ for a single-electrode transducer at the same frequency.

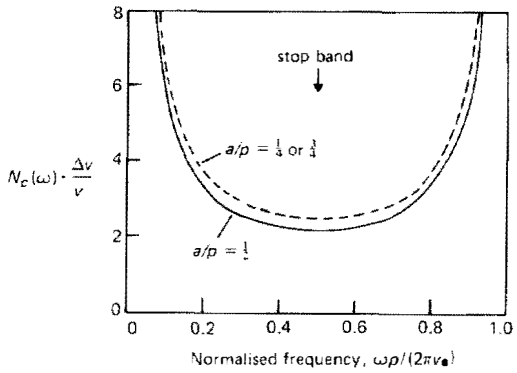

FIGURE 5.3. Number of electrodes for full transfer, as a function of frequency.

For a coupler of finite length, as in Figure 5.2, it is assumed that end effects are negligible, so that the above equations apply directly. The input and output wave amplitudes are measured at the centres of the first and last electrodes. It is assumed that a surface wave is incident in track A, and it is convenient to take $n = 0$ for the first electrode, since equation (5.27) gives $\phi_n^b = 0$ for $n = 0$, as required. The input wave amplitude, denoted ϕ_{i1}, is given by equation (5.26) with $n = 0$. The output wave amplitudes are denoted by ϕ_{t2} for track A and ϕ_{t4} for track B. Taking the number of electrodes to be $N + 1$, these are respectively given by equations (5.26) and (5.27) with $n = N$. It is convenient to relate the output amplitudes to the input amplitude by defining scattering coefficients S_{12} and S_{14}, so that

$$\equiv \qquad (5.29)$$

$$= \qquad - \qquad (5.30)$$

The magnitud $= \frac{1}{2}$. The solid

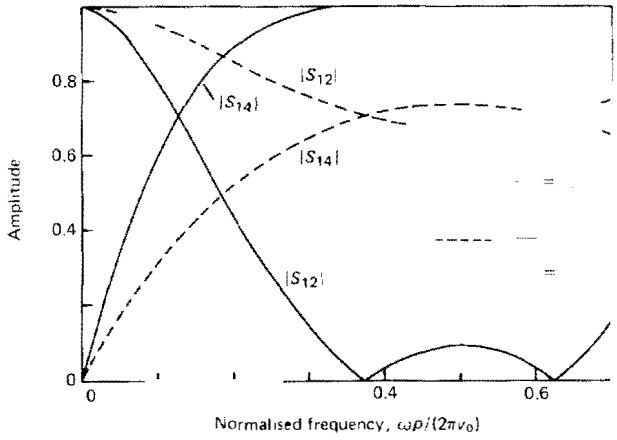

FIGURE 5.4 Scattering coefficients for simple couplers.

lines are drawn up for $N = 2.32/(\Delta v/v)$. This is equal to N_c when $\omega = 3\pi v_0/(4p)$, so all of the power emerges on track B at this frequency. In fact, the power transferred to track B varies little over a wide frequency range. Thus the coupler has a wide bandwidth, in contrast to a transducer with a comparable number of electrodes. The broken lines on Figure 5.4 refer to a coupler with half the number of electrodes, that is, with $N = 1.16/(\Delta v/v)$. In this case half of the power is transferred to track B at frequency $\omega = 3\pi v_0/(4p)$, so at this frequency the output amplitudes on the two tracks are the same. Such a coupler has a number of applications, discussed below, and is called a 3 dB coupler.

Coupler with Dissimilar Track Widths. The above analysis shows that a simple coupler can transfer all the surface-wave power from one track to the other if the appropriate number of electrodes is used. However, this is not true if the tracks have unequal widths. To illustrate this, we consider the coupler shown in Figure 5.5, where there are now three tracks. The electrodes in the outer tracks, tracks A and B, have the same pitch p and width a. Track C, in the centre, has angled electrodes so that the pitch, measured perpendicular to the electrodes, is different. This suppresses coupling to surface waves in track C, and is often used in practical devices in order to separate the active tracks and thus reduce cross-coupling due to diffraction spreading.

As before the analysis first assumes an infinite number of electrodes, and the results are then applied to a finite device. The electrode voltages in all three tracks are $V_n = V_0 \exp(-jn\kappa p)$, and continuity requires that the sum of the currents entering electrode n in the three tracks is zero. For tracks A and B the currents are given by equation (5.18), with W replaced by the track widths W_a or W_b, as appropriate. For track C there is no acoustic coupling, so the electrode currents I_n^c are given by

$$I_n^c/V_n = j\omega W_c C(\kappa), \tag{5.31}$$

where W_c is the electrode length in track C, as in Figure 5.5. The function $C(\kappa)$, given by equation (5.12), involves the constant ε_p^T, and this may have a value somewhat different to its value for the other tracks because of the anisotropy of the substrate.

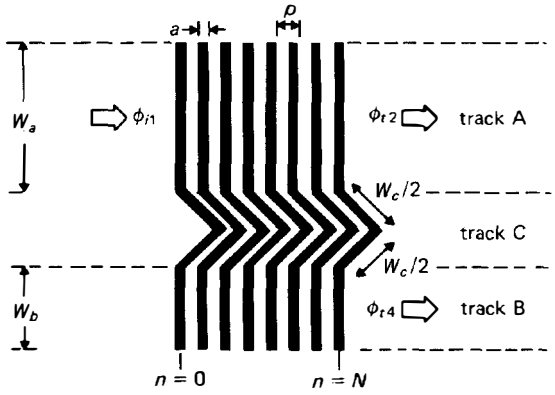

FIGURE 5.5. Coupler with unequal track widths.

However this may be allowed for simply by modifying the value of W_c in the equations.

As for the simple coupler described previously, it is found that there are two solutions for wave propagation in the infinite structure. One solution is obtained when the voltages V_n are zero, and from equation (5.18) this gives $\kappa = k_0 = k_{sc}$. The surface-wave potentials in tracks A and B are found using equation (5.15), and are related by $\phi_n^a W_a = -\phi_n^b W_b$. The other solution follows from equations (5.18) and (5.31), and gives a new solution for κ, here denoted by k_1. For this solution, $\phi_n^a = \phi_n^b$. For the finite structure of Figure 5.5 the two solutions are added, with one multiplied by a coefficient such that the total ϕ_n^b is zero for $n = 0$. Taking the number of electrodes to be $N + 1$, the output amplitude on track B is $\phi_{t4} = \phi_N^b$, and with $\phi_{i1} = \phi_0^a$ this is found to be given by

$$S_{14} \equiv \phi_{t4}/\phi_{i1} = \frac{2jW_a}{W_a + W_b} \sin(\tfrac{1}{2}\pi N/N_c') \exp(-jkNp), \tag{5.32}$$

where $k = (k_1 + k_{sc})/2$ and N_c' is given by

$$N_c'(\omega) = \frac{\pi}{p(k_{sc} - k_1)} = N_c(\omega)\frac{W_a + W_b + W_c}{W_a + W_b}, \tag{5.33}$$

where N_c is the number of electrodes for a full power transfer in a simpler coupler, given by equation (5.28). The surface-wave power in track B is thus maximised if the number of electrodes is equal to N_c'. However, not all the incident power is transferred to track B. From equation (3.34) of Chapter 3, the ratio of the output power on track B to the input power is $(W_b/W_a)|\phi_{t4}/\phi_{i1}|^2$, and equation (5.32) shows that this can be equal to unity only if $W_a = W_b$.

The amplitude of the output wave on track A is a more complicated expression, but for the particular case $W_a = W_b$ is given by

$$S_{12} \equiv \phi_{t2}/\phi_{i1} = \cos(\tfrac{1}{2}\pi N/N_c') \exp(-jkNp). \tag{5.34}$$

Thus, if tracks A and B have equal widths the coupler behaves in the same way as the simple coupler of Figure 5.2. A complete transfer of power from track A to track B is obtained if $N = N_c'$. In most practical cases W_c is smaller than W_a or W_b, so that N_c', given by equation (5.33), is not substantially larger than N_c.

Second-order Effects. Provided the frequency is not in or near any of the coupler stop bands, the above equations are found to agree well with experimental measurements [116, 121]. Some loss of power due to the resistivity of the electrodes is observed, and this was studied in detail by Maerfeld *et al.* [117, 118]. For a simple coupler (Figure 5.2), designed to transfer all the power from one track to the other, it was found that the loss is about 1 dB if the sheet resistivity of the electrodes (in ohms per square) is equal to $2500\lambda^2/W^2$, where λ is the wavelength. This formula assumes a Y, Z lithium niobate substrate, with $a/p = \frac{1}{2}$ and a frequency $\omega = 0.8\pi v_0/p$. A typical resistivity is 0.25 ohms per square, giving a 1 dB loss when the track width W is equal to 100 wavelengths. This is often the main cause of loss in practice. In addition

to the loss, the resistivity causes the output beam to have a variation of amplitude across the width of the track, though this is usually of little consequence if the loss is 1 dB or less.

Another possible cause of loss is the generation of bulk waves. From considerations of phase matching, it can be deduced that significant excitation of bulk waves can only occur for radian frequencies higher than $\pi v_0/p$. In practice the coupler is usually designed for operation at frequencies below this value, so bulk wave excitation is not significant. Further discussion is given in Appendix F.

Diffraction of the surface waves becomes relevant if the width of either track is only a few wavelengths. In this case the amplitude may vary with y in each track. The velocities of all the modes described above are less than the free-surface velocity v_0, and consequently the coupler has some characteristics in common with a waveguide. Experimental work [122] shows that the wave amplitude, as a function of y, has irregularities, and these can be predicted theoretically [123]. Diffraction can generally be ignored if the track widths are greater than 10 wavelengths.

For an input on track A, the coupler also produces reflected waves on both tracks. These will be ignored in this chapter. Some discussion is given in Appendix E, which shows that the reflections are generally negligible if the frequency is not close to one of the stop bands.

5.3. INTERDIGITAL DEVICES USING COUPLERS

In this section we consider the response of a device comprising two interdigital transducers and a multi-strip coupler, as in Figure 5.6. It will be shown that the device response is essentially the product of the two transducer responses, even if both transducers are apodised [124–126]. This feature is of considerable value in the design of sophisticated devices. Another important advantage is that the coupler reduces unwanted output signals due to the excitation of bulk waves by the input transducer; this is because any bulk wave incident in one track is coupled to the other track much less efficiently than a surface wave. Although this is clearly demonstrated

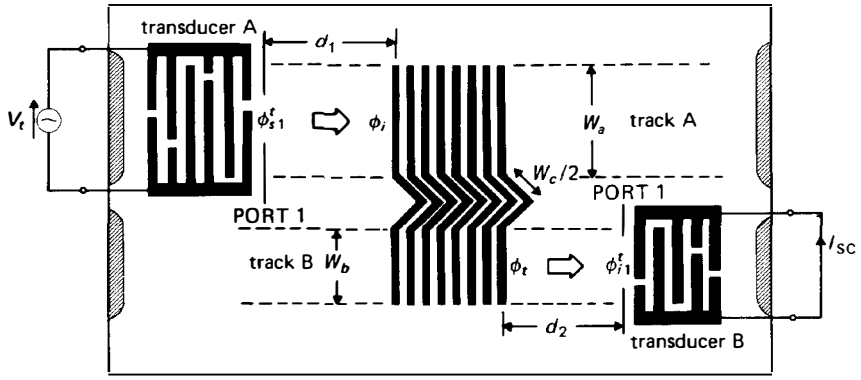

FIGURE 5.6. Interdigital device using a multi-strip coupler.

experimentally [126] it appears that a quantitative analysis has not been given. However, since bulk waves, observed at the surface, generally exhibit attenuation due to radiation into the bulk, it is clearly unlikely that the coupler could transfer bulk wave power efficiently from one track to another; furthermore, in practical devices the coupler is usually designed to optimise the coupling efficiency for surface waves.

For the analysis here, bulk wave excitation is ignored. As shown in Figure 5.6, the active region of each transducer is assumed to be confined within the appropriate track of the coupler, and the transducer apertures are taken to be equal to the coupler track widths W_a and W_b. It is assumed initially that transducer A is connected to a source with zero impedance, and transducer B is shorted. In this situation, the potential ϕ_t of the wave incident on the coupler in track A is a function of y, because transducer A is apodised. We show here that the amplitude of the output wave in track B can be found straightforwardly using superposition. Suppose first that a narrow beam of width Δy is incident, with amplitude $\phi_i(y_1)$ at the coupler input, where y_1 is the location of the centre of the beam. Assuming diffraction and electrode resistance to be negligible, the corresponding output wave must have an amplitude uniform across track B and its potential ϕ_t at the coupler output must be proportional to $\phi_i(y_1)$, so that

$$\phi_t = K\phi_i(y_1),$$

where the constant K is to be determined. Since electrode resistance is negligible the output wave amplitude is independent of the location y_1 of the input beam. Thus for a second input beam, centred at y_2 and with amplitude $\phi_i(y_2)$, the output amplitude is $\phi_t = K\phi_i(y_2)$. The total wave incident on the coupler is represented by J elementary beams, each of width Δy, and the total output wave is therefore, by superposition,

$$\phi_t = \sum_{j=1}^{J} K\phi_i(y_j).$$

This equation is still valid if all the $\phi_i(y_j)$ are equal, in which case $\phi_t = S_{14}\phi_i$, and since $J = W_a/\Delta y$ we conclude that $K = S_{14}\Delta y/W_a$. Taking the limit as $\Delta y \to 0$ we have

$$\phi_t = S_{14}\int_a \frac{\phi_i(y)}{W_a}\,\mathrm{d}y, \tag{5.35}$$

where S_{14} is given by equation (5.32) and the integral is taken over the width of track A. Thus the amplitude of the output beam is proportional to the average amplitude of the input beam.

The response of the overall device is now found with the aid of the transducer analysis of Chapter 4. The frequency responses of transducers A and B are respectively $H_t^a(\omega)$ and $H_t^b(\omega)$, both given by equation (4.128). In both cases, port 1 of the transducer is taken as the port nearest to the coupler. When a voltage V_t is applied to transducer A, the surface wave generated has potential $\phi_{s1}^t(y)$ at port 1, where the superscript t indicates a potential at one of the transducer ports. From the analysis of Section 4.7.2 we have

$$\int_a \phi'_{s1}(y)\,dy = jV_t W_a H_t^a(\omega)\left[\frac{\Gamma_s}{\omega W_a}\right]^{1/2}. \tag{5.36}$$

For transducer B, if a uniform surface wave beam of width W_b is incident, with potential ϕ'_{i1} at port 1, the short-circuit output current is

$$I_{sc} = -j\phi'_{i1}[\omega W_b/\Gamma_s]^{1/2} H_t^b(\omega). \tag{5.37}$$

Taking d_1 as the separation between transducer A and the coupler, and d_2 as the separation between transducer B and the coupler, the above equations give the overall device response as

$$H_{sc}(\omega) \equiv I_{sc}/V_t = H_t^a(\omega)H_t^b(\omega)S_{14}(W_b/W_a)^{1/2}\exp[-jk_0(d_1 + d_2)], \tag{5.38}$$

which is essentially the product of the two transducer responses and the coupler response S_{14}, which varies slowly with frequency. This approach is valid only if reflected waves are insignificant, that is, if electrode interactions in the transducers are negligible, and if the frequency is not close to one of the coupler stop bands.

For finite source and load impedances the frequency response is modified somewhat by the circuit effect and the transducers reflect the waves, giving a triple-transit spurious signal. These features can be calculated using the analysis of Section 4.8, which is sufficiently general to allow for the presence of the coupler. Thus the main response of the device is given by equation (4.137), and the triple-transit response is given by equation (4.147); in both cases, equation (5.38) is used for the short-circuit response $H_{sc}(\omega)$.

5.4. UNIDIRECTIONAL TRANSDUCER

A 3 dB coupler may be used to modify a conventional bidirectional transducer in such a way that it becomes essentially unidirectional. As shown in Figure 5.7(a), the

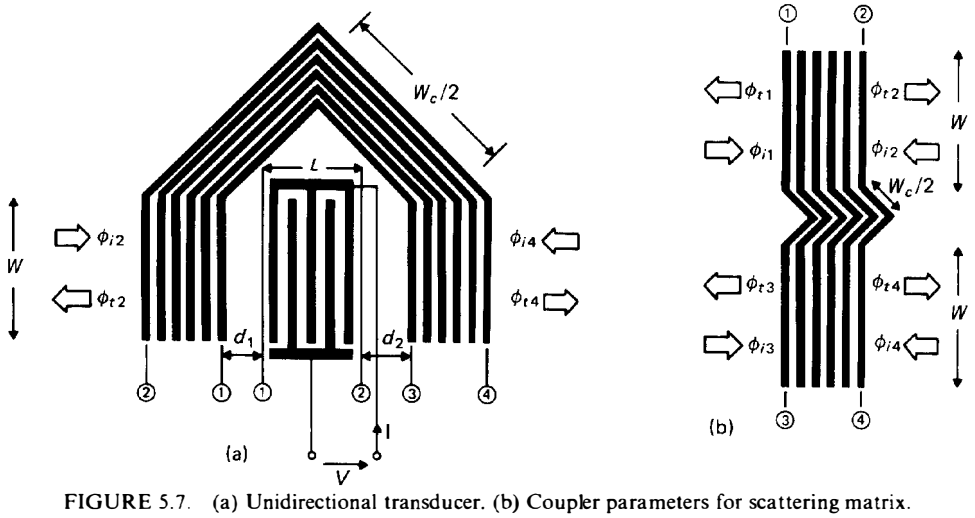

FIGURE 5.7. (a) Unidirectional transducer. (b) Coupler parameters for scattering matrix.

coupler is folded into a "U"-shape, and a symmetrical unapodised transducer is located between the parallel arms of the coupler. When a voltage is applied, the surface wave leaving the coupler at the right is the sum of two components, arising from the waves launched to left and right by the transducer. These two components cancel if the coupler provides 3 dB coupling and if the transducer is displaced slightly to the left, so that the waves arrive at the coupler inputs in phase quadrature. Thus, surface waves emerge only at the left. By reciprocity, a wave incident from the left will not be reflected provided the transducer is matched, and this feature is useful for minimising the triple-transit spurious signal in surface wave devices. However, the behaviour is strictly unidirectional only at one particular frequency.

For the analysis it is convenient to define a scattering matrix for the coupler. As shown in Figure 5.7(b), we consider a coupler whose acoustically-coupled tracks have equal apertures W, and denote the four inputs as ports 1 to 4. The potentials of incident surface waves are denoted by ϕ_i and those of surface waves leaving the coupler by ϕ_t. In each case these are also subscripted 1, 2, 3 or 4 to identify the port. For a wave incident from the left in one track, the output waves are given by equations (5.32) and (5.34), while for other incident waves the outputs are obtained by symmetry. The scattering matrix may therefore be written as

$$\begin{bmatrix} \phi_{t1} \\ \phi_{t2} \\ \phi_{t3} \\ \phi_{t4} \end{bmatrix} = \begin{bmatrix} 0 & S_{12} & 0 & S_{14} \\ S_{12} & 0 & S_{14} & 0 \\ 0 & S_{14} & 0 & S_{12} \\ S_{14} & 0 & S_{12} & 0 \end{bmatrix} \begin{bmatrix} \phi_{i1} \\ \phi_{i2} \\ \phi_{i3} \\ \phi_{i4} \end{bmatrix}, \tag{5.39}$$

where the coefficients are

$$S_{12} = \cos\left(\tfrac{1}{2}\pi N/N_c'\right) \exp\left(-jkNp\right), \tag{5.40}$$

$$S_{14} = j \sin\left(\tfrac{1}{2}\pi N/N_c'\right) \exp\left(-jkNp\right). \tag{5.41}$$

Here N is the number of electrodes, N_c' is given by equation (5.33), and $k = (k_1 + k_{sc})/2$. In equation (5.39) it is assumed that reflected waves can be ignored so that, for example $S_{11} = S_{31} = 0$. This is a reasonable assumption provided the frequency is not in or near one of the coupler stop bands. Strictly speaking, the analysis of the coupler in the unidirectional transducer, Figure 5.7(a), should allow for the fact that the acoustically inactive parts of the electrodes vary in length. However this is not found to change its behaviour appreciably, so the above scattering matrix can be applied, taking W_c as the average of the electrode lengths in the inactive region.

The transducer behaviour is described by the scattering matrix already given in Section 4.4, equation (4.79). To distinguish this from the coupler scattering matrix, the elements of the transducer matrix are here written as S_{ij}'. Since the transducer is symmetrical, its electrostatic charge density $\varrho_e(x)$ is also symmetrical, and it follows that $\tilde{\varrho}_e(k_0)$ is real. We thus have $S_{13}' = S_{23}' = -S_{31}' = -S_{32}'$. The transducer scattering matrix is combined with the coupler scattering matrix, equation (5.39), to give a scattering matrix for the unidirectional transducer. This is denoted by S_{ij}', and defined by

$$\begin{bmatrix} \phi_{t2} \\ \phi_{t4} \\ I/(\omega W) \end{bmatrix} = \begin{bmatrix} S'_{11} & S'_{12} & S'_{13} \\ S'_{21} & S'_{22} & S'_{23} \\ S'_{31} & S'_{32} & S'_{33} \end{bmatrix} \begin{bmatrix} \phi_{i2} \\ \phi_{i4} \\ V\Gamma_s \end{bmatrix}, \tag{5.42}$$

where I and V are the transducer current and voltage, as shown on Figure 5.7(a). Defining d_1 as the distance between the coupler port 1 and the transducer port 1, and d_2 as the distance between the coupler port 3 and the transducer port 2, the matrix elements in equation (5.42) are found to be

$$\begin{aligned} S'_{11} &= S'_{22} = 2S'_{12}S_{12}S_{14}\exp[-jk_0(d_1+d_2)] \\ S'_{12} &= S'_{21} = S'_{12}(S^2_{12}+S^2_{14})\exp[-jk_0(d_1+d_2)], \\ S'_{13} &= -S'_{31} = [S_{12}\exp(-jk_0d_1)+S_{14}\exp(-jk_0d_2)]S'_{13}, \\ S'_{23} &= -S'_{32} = [S_{14}\exp(-jk_0d_1)+S_{12}\exp(-jk_0d_2)]S'_{13}, \\ S'_{33} &= S'_{33} = Y_t(\omega)/(\omega W\Gamma_s), \end{aligned} \tag{5.43}$$

where $Y_t(\omega)$ is the admittance of the transducer in the absence of the coupler.

The coupler is designed to give 3 dB coupling at a frequency ω_c, which is the transducer centre frequency. At this frequency $N = \frac{1}{2}N'_c$, and $S_{14} = jS_{12}$. The transducer is displaced to the left by a small precise amount, such that $(d_2 - d_1)$ equals one quarter-wavelength at frequency ω_c, and hence $\exp[-jk_0(d_1 - d_2)] = j$. It follows that at this frequency S'_{23} is zero, and hence when a voltage is applied to the transducer there is no wave emerging at the right. It is also found that for a wave of frequency ω_c incident on port 2 there is no reflected wave if the transducer is electrically matched, that is, if it is connected to a load whose admittance is equal to $Y_t^*(\omega_c)$, the conjugate of the transducer admittance.

Figure 5.8 shows the reflection coefficient for surface waves incident on port 2 of the coupler, and the conversion coefficient for waves leaving port 2. The latter is the

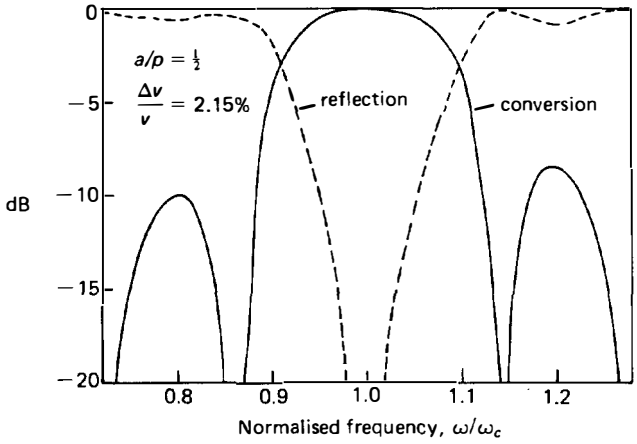

FIGURE 5.8. Reflection and conversion coefficients for a unidirectional transducer.

ratio of the surface wave power to the power available from a generator connected to the transducer. The transducer is taken to be of the uniform single-electrode ($S_e = 2$) type, with $N_p = 7$ periods, and its admittance is given by equations in Section 4.6. The electrical load is, as in common practice, a series inductor followed by a fixed resistance, with values chosen to match the transducer impedance at the centre frequency ω_c. The coupler is designed to give 3 dB coupling at frequency ω_c, and its electrodes have pitch p such that $\omega_c = 3\pi v_0/(4p)$. It can be seen that at the transducer centre frequency ω_c the conversion coefficient is 0 dB, and incident waves are not reflected. In contrast, a matched bidirectional transducer theoretically gives a conversion coefficient of 3 dB and a reflection coefficient of 6 dB, as shown in Section 4.4.4. Thus the unidirectional transducer is much superior at the centre frequency. On the other hand, the reflection coefficient is quite large at the edges of the transducer pass-band, for reasons discussed below. Thus the unidirectional transducer is best suited for applications where the signal bandwidth is less than the transducer bandwidth.

Experimental measurements give results similar to Figure 5.8, though generally with a few dB's of loss due mainly to the resistance of the electrodes in the transducer and in the coupler. For example [126] a transducer centred at 61 MHz gave a minimum conversion loss of 1.5 dB, and a delay line comprising two such transducers had an insertion loss of 3 dB.

5.5. OTHER APPLICATIONS OF 3 dB COUPLERS

Two further applications of 3 dB couplers are shown in Figure 5.9. On the left is a multi-strip *mirror*, an efficient reflector of surface waves. This comprises a 3 dB coupler folded into a "U"-shape, and is thus similar to a unidirectional transducer [Figure 5.7(a)] except that the transducer has been omitted. The reflection coefficient at port 2 can be obtained from the coupler scattering matrix of equation (5.39); alternatively, it can be obtained from the scattering matrix of a unidirectional transducer, equation

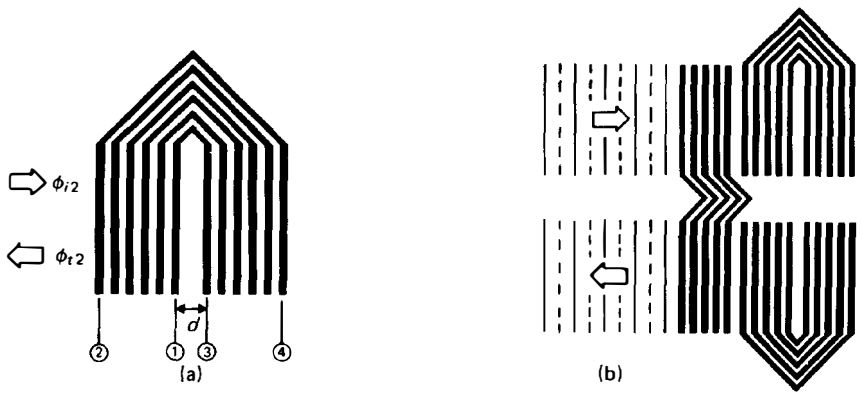

FIGURE 5.9. (a) Multi-strip mirror, (b) reflecting track-changer.

(5.42), setting $V = 0$. Thus, if there are no waves incident on port 4 the mirror gives

$$\phi_{t2}/\phi_{i2} = S'_{11} = j \sin(\pi N/N'_c) \exp[-j(2kNp + k_0 d)], \qquad (5.44)$$

where d is the distance between ports 1 and 3, as in Figure 5.9(a), N is the number of electrodes and N'_c is given by equation (5.33). For a 3 dB coupler we have $N = \frac{1}{2}N'_c$ so that the magnitude of the reflection coefficient is unity. Further, N'_c is almost independent of frequency, so that the reflection coefficient is close to unity over a wide band. Experimental results [126] centred at 80 MHz demonstrate a reflection loss constant within about $\frac{1}{4}$ dB over a bandwidth exceeding 60%; however the loss is about 2 dB, which can be attributed to electrode resistance [118]. The operation of the mirror explains why the reflection coefficient of a unidirectional transducer is close to unity except near the centre frequency, as seen on Figure 5.8. For frequencies remote from the centre frequency the transducer has litte effect on any incident surface wave, and the unidirectional transducer thus behaves like a mirror, enhancing the reflection coefficient instead of reducing it.

Figure 5.9(b) shows a *reflecting track-changer* which, in response to an input surface wave beam, generates an oppositely directed beam on an adjacent track. This device has a straight 3 dB coupler followed by two mirrors. The straight coupler partitions the input wave equally between the two mirrors, and the reflected waves pass through the straight coupler for a second time. Apart from the change of direction this process is equivalent to passage through two 3 dB couplers in cascade, and hence ideally all the power emerges in the output track. As in the case of the mirror alone, the output power varies very slowly with frequency. Experimentally [126] a loss of 2 to 3 dB was obtained, over a bandwidth exceeding 50%. The track-changer may be used in a surface-wave delay line to increase the delay obtainable for a given length of substrate. In fact, by using track-changers at both ends of the substrate the surface wave may be made to traverse the substrate length several times. A device with eight track-changers gave 130 μsec delay and 23 dB insertion loss [127].

Several other multistrip devices are described by Marshall *et al.* [126], including an "echo trap". This reduces triple-transit signals more effectively than a unidirectional transducer, but gives somewhat greater losses. Maerfeld *et al.* [117] investigated the effect of electrode resistance in a variety of devices, including novel types of trackchanger. Chapman and Bristol [128] have shown that the performance of some of these devices may be improved if slightly different pitches are used for the electrodes in the two tracks.

5.6. BANDPASS FILTERING USING MULTI-STRIP COUPLERS

The multi-strip devices described so far have wide bandwidths. There are however several methods of obtaining a narrower bandwidth, with potential application to bandpass filtering. In a technique introduced by Solie [129] the electrodes in one track are displaced in groups in the direction of surface wave propagation, as shown in Figure 5.10(a). The displacements introduce phase shifts in the waves launched in the output track by individual groups of electrodes. Denoting the displacements by d_i, as in Figure 5.10(a), the overall response can be written approximately as

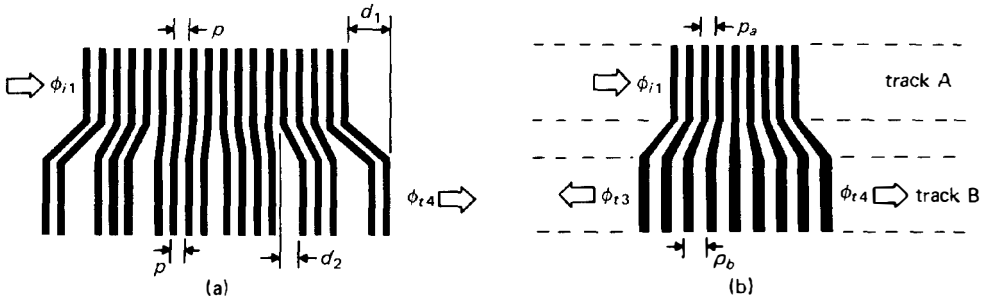

FIGURE 5.10. Narrow-band multi-strip couplers for bandpass filtering.

$$\phi_{t4}/\phi_{i1} \approx \sum_i A_i \exp\,[jk_0(d_i - Np)], \tag{5.45}$$

where the coefficients A_i give the amplitudes of the waves generated by individual electrode groups. It is a reasonable approximation to take the A_i to be independent of frequency, in which case equation (5.45) has the form of the response of a transversal filter. Standard techniques, described in Chapter 8, may then be used to deduce appropriate values for the A_i and d_i, such that the response approximates some required response. In practice, this method is somewhat inflexible because the experimental A_i-values are controlled only by varying the numbers of electrodes in individual groups, and the accuracy is affected by end effects. However this disadvantage is offset by the fact that the coupler can be combined with weighted transducers, and in addition the loss can be very low. Solie [129] instances a coupler with a 3 dB bandwidth of 9 MHz centred at 213 MHz, with 3 dB loss at the centre frequency and 30 dB out-of-band rejection.

Another technique for narrow bandwidths is the use of different electrode pitches in the two tracks, as shown in Figure 5.10(b). In this structure, strong coupling between propagating surface waves in the two tracks can occur only if their phases, observed at the electrode locations, are equal or differ by a multiple of 2π. Taking p_a and p_b as the electrode pitches in tracks A and B respectively, and noting that the wavenumber must be close to k_0, the phase matching condition is

$$p_b \pm p_a \approx 2\pi m/k_0, \tag{5.46}$$

where m is an integer. The upper sign applies for waves propagating in opposite directions in the two tracks, and the lower sign for waves propagating in the same direction. For a wave incident in track A, the response observed in track B is a narrow-band function, with bandwidth related to the number of electrodes and with centre frequency given by equation (5.46). For either output port, the amplitude, as a function of frequency, is observed [129] to have the form of the function $(\sin x)/x$. Several methods of introducing weighting are described by Feldmann and Henaff [130]. In particular, the electrodes in track B may be fanned out so that the pitch varies across the track, increasing the bandwidth over which efficient coupling occurs. In this case waves are generated in track B at locations dependent on the frequency. An array

of output transducers may be used, so that different frequency components emerge from different output transducers, and the device is then a filter bank. A device with five outputs, each with about 2 MHz bandwidth, was demonstrated. Another type of filter bank, using 3 dB couplers, is described in Chapter 8.

5.7. BEAM COMPRESSION

Another modification of the basic coupler geometry can be introduced in order to couple efficiently two tracks with different widths. As shown in Section 5.2, some power loss occurs if the electrodes are identical in the two tracks; however efficient coupling can be obtained if the pitches are slightly different [131], as shown in Figure 5.11(a). This technique has been used in surface-wave convolvers, where the enhancement of power density due to the compression of the beam leads to an improvement in device efficiency. It is also of interest for efficient coupling of transducers with different apertures.

The device can be analysed using equations in Section 5.1 above. The metallisation ratio is taken to be the same in all three tracks. Taking p_a and p_b as the pitches in tracks A and B, the electrode voltages can be written as $V_n = V_0 \exp(-jn\kappa_a p_a)$ for track A and $V_n = V_0 \exp(-jn\kappa_b p_b)$ for track B. These must of course be equal, so that we can write

$$\kappa_a p_a = \kappa_b p_b = \gamma.$$

The voltages are also equal if a multiple of $2\pi/p_b$ is added to κ_b, but this is not of interest here. The currents entering the electrodes in the three tracks are given by equation (5.18), which involves the slowly-varying functions $C(\kappa)$ and $\bar{\varrho}_f(\kappa)$, dependent on κ and p. The solutions of interest here have κ close to k_0, and the pitches in the three tracks are closely similar, so these functions can be taken as $C(k_0)$ and $\bar{\varrho}_f(k_0)$ in all tracks, using an average value of the pitch. Using equation (5.18) and setting the sum of the currents entering the three tracks to zero shows that there are two positive solutions for γ, denoted by γ_+ and γ_-, and these are related to the pitches p_a and p_b and the track widths W_a, W_b and W_c. The surface wave amplitudes in tracks A and B for these two modes are given by equation (5.19). The two modes are added, with an amplitude ratio such that the total surface wave potential in track B is zero for $n = 0$, the left end of the coupler. If the coupler is to transfer all the power from

FIGURE 5.11. Beam compression.

track A to track B, it is also necessary that the wave amplitude in track A should be zero for some $n \neq 0$. This is found to give a further relationship between $\gamma_{\pm}$ and the pitches p_a and p_b. After some manipulation, it is found that the required relationship between the pitches is

$$p_a - p_b = \frac{\pi}{k_0 N_c} \frac{W_a - W_b}{W_a + W_b + W_c} \tag{5.47}$$

and, if this relation is satisfied, a complete transfer of power from one track to the other is obtained if the number of electrodes is N_c', given by

$$N_c' = N_c \frac{W_a + W_b + W_c}{2\sqrt{W_a W_b}} . \tag{5.48}$$

In these equations, N_c is the number of electrodes required for a complete transfer in a simple coupler, given by equation (5.28). Equation (5.48) shows that the number of electrodes required is quite practicable, even for quite large ratios of track widths; for example, a 10:1 ratio of track widths requires about 190 electrodes on a Y, Z lithium niobate substrate. The required difference between the pitches, equation (5.47), is typically 1%. Experimental results [131] generally show good agreement for track width ratios up to 15:1, though a loss of up to about 1 dB is observed, due to the resistance of the electrodes. However, larger losses, due to surface wave diffraction, are found if the width of the narrower track is less than about five wavelengths.

An alternative type of multi-strip beam compressor makes use of 3 dB couplers [126], as illustrated in Figure 5.11(b). It was seen in Section 5.4 that for a 3 dB coupler the scattering coefficients S_{12} and S_{14} are of equal magnitude and are in phase quadrature. In the beam compressor an additional $\pi/2$ phase change is introduced by displacing the electrodes in one track by a quarter-wavelength relative to the other track. For incident waves of equal amplitude and phase on both tracks, this causes the output on one track to be cancelled, and thus an input beam spanning both tracks has its width reduced by a factor of two. Additional couplers can be used to provide further width reduction. Using three couplers a width compression of 8:1 was demonstrated [126], with only 0.5 dB of loss. In comparison with the device of Figure 5.11(a), this method generally requires a larger number of electrodes for a given compression ratio and is also rather more frequency-dependent, since the electrode displacement gives the required phase change only at one particular frequency.